Appl Biochem Biotechnol (2011) 163:792–802
DOI 10.1007/s12010-010-9083-0

Plant Oil Bodies: Novel Carriers to Deliver Lipophilic Molecules

Stefania Bonsegna · Simona Bettini · Rosanna Pagano · Antonella Zacheo · Viviana Vergaro · Giovanna Giovinazzo · Gabriella Caminati · Stefano Leporatti · Ludovico Valli · Angelo Santino

Received: 23 April 2010 / Accepted: 7 September 2010 /
Published online: 18 September 2010

Abstract Oil bodies (OBs) are specialised organelles ubiquitously detected in plant oil seeds, which serve as lipid storage compartments. OBs consist of a hydrophobic core of triacylglycerol (TAGs), surrounded by a monolayer of phospholipids (PLs) embedded with some specific proteins with a size ranging from 0.5 to 2 μm. In this work, we report an easy method to reconstitute OBs starting from their constituents and to encapsulate lipophilic molecules, i.e. the fluorescent fluorescein isothiocyanate (FITC) and carboxyfluorescein (CF), into reconstituted OBs. This methods allowed us to produce OBs 4- to 10-fold smaller (50–200 nm) than the native one and to obtain a good recovery (about 40%) of both the fluorescent compounds used in the present work. The properties of reconstituted OBs were investigated by a combination of Brewster angle microscopy, scanning force microscopy, ζ-potential techniques. OBs were stable and formed ordered monolayers when patterned on hydrophobic substrates whereas they showed a higher tendency to aggregate into larger, coalescing OBs when were deposited onto hydrophilic substrates or at the air/water interface. Furthermore, we verified the uptake of FITC-loaded OBs by the MCF-7 breast cancer cell line. Our results indicated that OBs could be envisaged as novel carriers to deliver hydrophobic bioactive compounds.

Keywords AFM analysis · Air/water interface characterization · Cellular uptake · Langmuir–Schaefer films · MCF-7 cells · Oil bodies

Stefania Bonsegna and Simona Bettini contributed equally to this work.

S. Bonsegna · G. Giovinazzo · A. Santino (✉)
Institute of Sciences of Food Production CNR Unit of Lecce, Via Monteroni, 73100 Lecce, Italy
e-mail: angelo.santino@ispa.cnr.it

S. Bettini · R. Pagano · L. Valli
Dipartimento di Ingegneria dell'Innovazione, Università del Salento, 73100 Lecce, Italy

A. Zacheo · V. Vergaro · S. Leporatti
NNL-Nanoscience Institute of CNR Lecce, IIT Research Unit, Via Arnesano, 73100 Lecce, Italy

G. Caminati
Department of Chemistry and CSGI Consortium, University of Florence, Via della Lastruccia, 3 50019 Sesto Fiorentino, Florence, Italy

Introduction

Plant seeds store triacylglycerols (TAGs) into oil bodies (OBs), specialised organelles which serve as an energy reserve during germination and post-germinative growth. OBs consist of a hydrophobic core of TAGs, surrounded by a monolayer of phospholipids (PLs) embedded with some specific proteins, including oleosins and some minor proteins, i.e. caleosin and steroleosin [1–6]. OBs from different plant species commonly consist of 98–94% TAGs, 0–5–2% PLs and 0.5–3.5% proteins and show a size ranging from 0.5 to 2 μm, as visualised in the schematic representation of plant OBs shown in Fig. 1a.

Due to the easy purification procedures from plant seeds and the possibility of obtaining artificial OBs starting from recombinant oleosin or caleosin [7, 8], there is an increasing interest to use them as nanocarriers to deliver pharmaceutical drugs or foreign proteins and peptides of therapeutic interest via their expression as fusions with oleosin or other OBs proteins [1–3]. The interfacial behaviour of the single components of OB has been studied in the past [9–11]. However, to our best knowledge, the behaviour and stability of OBs at air/water interface or when patterned onto different surfaces have not yet been investigated. This information could be of primary importance for future pharmaceutical applications of OBs.

In the present work, we report an easy method to reconstitute natural OBs starting from their constituents and to encapsulate lipophilic molecules, i.e. the fluorescent fluorescein isothiocyanate (FITC) and carboxyfluorescein (CF), into reconstituted OBs. This method allowed us to produce OBs 4- to 10-fold smaller (50–200 nm) than the native ones and to obtain a good recovery (about 40%) of both the fluorescent compounds used in the present work.

The properties of reconstituted OBs were investigated by a combination of different techniques. Finally, we verified the uptake of FITC-loaded OBs by the MCF-7 breast cancer cell line.

Experimental

Chemicals

The chemicals used for this study are as follows: penicillin–streptomycin solution (Sigma, USA), sodium pyruvate (Sigma, USA), Dulbecco's modified Eagle medium

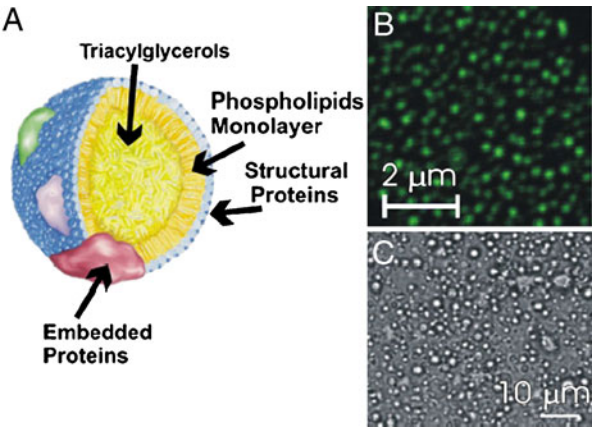

Fig. 1 **a** Schematic representation of a plant OB. **b** Fluorescent OBs imaged by Confocal Laser Scanning Microscopy (CLSM). **c** Native OBs visualised by transmitted light

(DMEM) medium (Sigma, USA), thiazolyl blue tetrazolium bromide ≥97.5% TLC (Sigma, USA), phosphate-buffered saline (PBS), Dulbecco A (PBS, Oxoid), triton X-100 (Sigma, USA), FITC (Sigma, USA) and CF (Sigma, USA).

Purification of seed OBs and Reconstitution with FITC and Carboxyfluorescein

Seed OBs were purified from hazelnut and almond seeds by two-layer flotation as previously reported [12], and further purified by two sequential washings with 2.0 M NaCl and finally resuspended in 150 mM Tris–HCl, pH 7.5, containing 0.6 M sucrose.

FITC-loaded OBs were prepared starting from 500 mg OBs. They were extracted twice with ten volumes of chloroform/methanol (2:1, v/v). After centrifugation at 1,000×*g* for 5 min, the lower chloroform/methanol phase was dried. The upper phase was extracted twice with ten volumes of hexane and the solvent completely evaporated. OBs were reconstituted using both the chloroform/methanol and the hexane extracts in the presence of different amounts (0.5, 1, 2 mg) of FITC or CF (purchased by Sigma). The suspension was sonicated using a standard ultrasonicator bath for different times (30, 60, 120 min). At the end, the reconstituted OBs were resuspended in grinding buffer, centrifuged and recovered from the top of the tube. Three further washing steps were carried out to remove the excess of FITC or CF.

Confocal Laser Scanning Microscopy

Fluorescent OBs were imaged by confocal microscopy using an excitation wavelength of 488 nm. The emission was recorded with the 505–530 nm filter set. Confocal micrographs of intracellular uptake were taken with a Leica confocal scanning system mounted to a Leica TCS SP5 (Leica Microsystem GmbH, Mannheim, Germany) and equipped with a 63× oil immersion objective.

Imaging by Scanning Force Microscopy

Scanning force microscopy (SFM) imaging was conducted using a Multimode-Picoforce system (Veeco Instruments Inc., Santa Barbara, CA, USA). OBs were imaged after deposition onto silicon substrates (hydrophilic and hydrophobic) at room temperature in air in tapping mode. For tapping mode imaging we used RFESPA silicon cantilevers (Veeco Instruments Inc.) of about 3 N/m spring constant with a resonance frequency of around 80 kHz. Topographical (height), Amplitude and Phase images are acquired in at least three different position. Representative Amplitude images are selected because are showing higher details of OBs morphology. Size and thickness measurements were performed on corresponding height images by using Nanoscope Software (version 6.14r1).

The sensitivity of the optical system was calibrated and the cantilever spring constant determined prior to each experiment using built-in routines of the manufacturer (Nanoscope IIIa version 6.14r1). Specifically, the optical lever sensitivity (necessary to convert the voltage applied to the piezo into tapping mode deflection distance of the cantilever in nanometers) was determined on a bare glass substrate from force-vs.-distance curves taken at 0.5 Hz. The cantilever spring constant was measured using the thermal noise method [13, 14].

Langmuir–Schäfer Deposition

Experiments were carried out by a NIMA 601 LB apparatus. Ultrapure water (Millipore Milli-Q, 18.2 MΩ cm) was used as the solvent for the sub-phase: the pH of the water solution sub-phase, containing KCl 100 mM, K-phosphate 10 mM and sodium acetate 5 mM, was regulated by carefully controlled additions of KOH or HCl solutions. The temperature of the sub-phase was regulated at 20 °C by a Haake GH-D8 apparatus. OB suspensions were resuspended in an aqueous medium of the same composition as the sub-phase; different volumes (in the range of 100–500 μL) of the OB suspensions were injected by a gastight syringe into the sub-phase depending on the trough size. The surface pressure was simultaneously monitored by a Wilhelmy balance in order to register the kinetics curves.

The surface layer was transferred via the Langmuir–Schäfer (LS) deposition technique onto different substrates (hydrophilic or hydrophobised silicon/silicon dioxide plates). Hydrophobisation was conducted by exposure for 24 h to a saturated atmosphere of 1,1,1,3,3,3-hexamethyldisilazane (HMDS). The transfer was performed at the surface pressure in the plateau region of each kinetics curve by lowering the substrate horizontally until contact with the floating film [15, 16].

ζ Potential Measurements

The ζ-potential values for the seed OBs purified from hazelnuts and almonds and for artificial OB were determined at pH values from 7 to 4.

ζ-potential was determined by a Zetasize Nano-ZS90 (Malvern Instruments Ltd, Malvern, UK) that uses a combination of laser Doppler velocimetry and phase analysis light scattering (PALS) in a technique called M3-PALS to measure particle electrophoretic mobility in an applied electric field. The samples, diluted in 10 mM sodium phosphate buffer at selected pH values (ranging from 4 to 7), were injected into a cell where a potential is applied. ζ-potential is related to the electrophoretic mobility by the Henry equation [17]. The ζ-potential is reported as the average and standard deviation of measurement calculated from three freshly prepared samples, with two readings for each sample.

Cell Culture

Human epithelial carcinoma cell line (HeLa) and human breast cancer cell line (MCF-7) were maintained in DMEM medium supplemented with FBS (10%), penicillin (100 U/ml culture medium), streptomycin (100 μg/ml culture medium), glutamine (5%) and sodium pyruvate (5%). Cells were grown in a humidified incubator at 37 °C, 5% CO, and 95% relative humidity. MCF-7 cells were fixed in 3.7% formaldehyde in PBS for 5 min, permeabilized with Triton X-100 (0.1% in PBS) followed by a 30 min incubation at room temperature with phalloidin-TRITC (Sigma). HeLa cells were then washed with PBS for 5 min and subsequently stained with 1 μg/ml of Hoechst 33342 for 5 min at room temperature.

Cellular Uptake

To determine the cellular uptake of OBs, we seeded 10^5 cells/ml in sterile glass-culture slide coating with poly-L-Lysine. The cells were incubated with the OBs dispersion. After 4 h of incubation at 37 °C, the culture medium was removed, the cells were washed three times with PBS with Ca^{2+} and Mg^{2+}. Then new medium was added to cell culture.

Result and Discussion

Encapsulation of Lipophilic Drugs Into Reconstituted OBs

In order to demonstrate that plant OBs could have potential applications as micro/nanocariers to deliver hydrophobic drugs, we reconstituted OBs using a method similar to that already reported for the reconstitution of artificial OBs [7, 8], but starting from their native constituents, namely triacylglycerols (TAG), phospholipids (PL) and structural proteins which were recovered either in the methanol/chloroform or the hexane fractions. Using the above-described protocol, we were able to reconstitute OBs of a similar shape to the natural ones. As far as the size of the reconstituted OBs is concerned, it was influenced by the length of the sonication step since longer sonications resulted in larger OBs (data not shown). The present work was carried out on smaller reconstituted OBs, obtained with a sonication step of 60 min, whose size ranged from 50 to 200 nm (Fig. 1b, and the following results shown in Fig. 2), since such a size is considered more useful for drug delivery mediated by micro/nanocapsules.

As proof of the reported successful procedure, FITC or CF, two fluorescent hydrophobic compounds, were encapsulated into reconstituted OBs (Fig. 1b) and compared with native OBs (Fig. 1c). Using this protocol, a recovery of about 40% of each compound (starting from 1 mg) was obtained.

OB Monolayers Morphology

OBs at the air/water interface were transferred by LS method onto solid support using both hydrophilic and hydrophobic substrates. Figure 2 shows amplitude SFM images of the resulting OBs "monolayer" deposited onto hydrophilic (a) and hydrophobic silicon substrate (b). All images were acquired in air immediately after their deposition. SFM images revealed a strong tendency to coalesce into larger structures for OBs deposited onto hydrophilic silicon substrates (see patches in Fig. 2a). After/during adhesion onto this substrate they are not stable enough to maintain their shape and open and fuse together (see round-shaped "islands") into patched structures (see irregular structure of more than 1 μm in size selected in the section in Fig. 2a at the bottom), which however, maintain a thickness similar to that of a single OB as visualized by Z-profile shown in the insets of Fig. 2a and b, thus indicating that they derived from several single OB coming together and leading to a flattened coalescing structures once they adhere onto the hydrophilic silicon substrate.

By converse, OBs deposited onto a hydrophobic support, appeared more stable and maintained their original quasi-spherical shape (Fig. 2b), in this case the presence of a hydrophobic functionalization of the silicon surface had the twofold advantage of ensuring a better transfer of the phospholipid monolayer matrix and to prevent the polar OB head groups to interact with the solid surface, a phenomenon that would lead to single OBs rupture and aggregation as observed on hydrophilic silicon. As shown in the inset of Fig. 2b, height peaks widths in the Z-profile are due to spherical OBs of different sizes. They range between 50 nm (i.e. shorter peak in the Z-profiles, as in the inset of Fig. 2b) and about 200 nm (i.e. the highest peak in the section of Fig. 2b, inset). SFM allows us to investigate fine nanostructures in OBs, going down to few hundred nanometers scan sizes. Figure 2c and d shows higher magnification Amplitude images (2×2 μm and 1×1 μm scan areas) of OBs deposited onto hydrophobic substrates. They are rather monodisperse, covering almost homogeneously the whole surface and having a typical spherical shape.

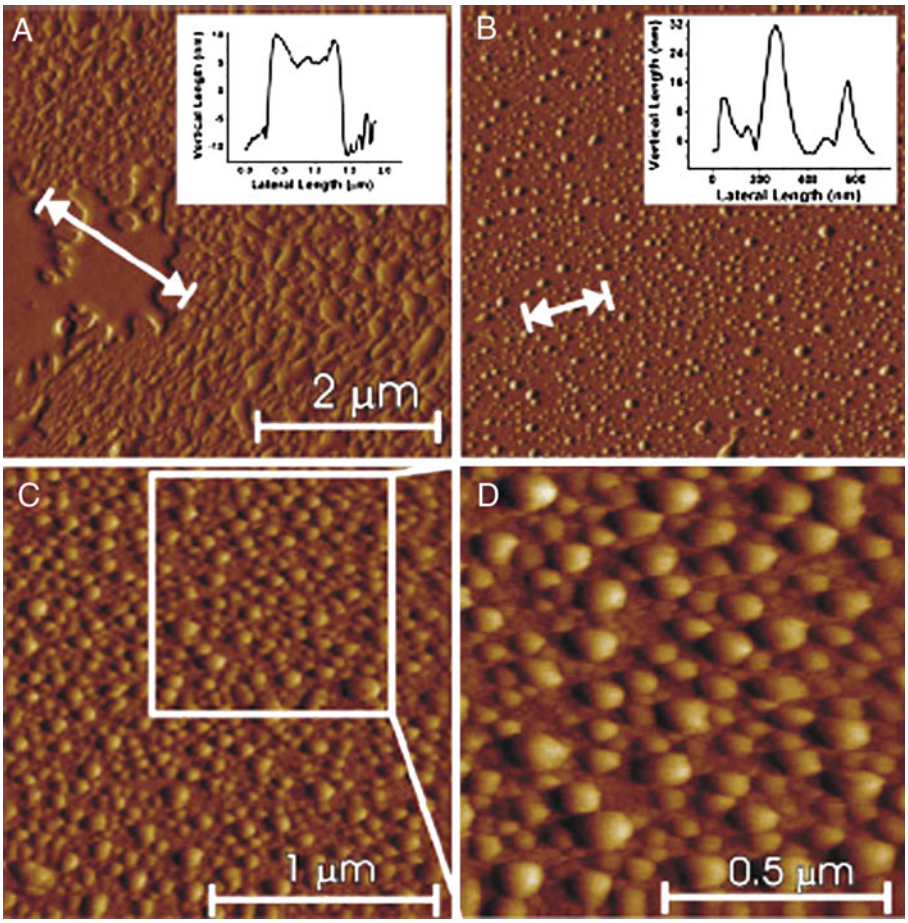

Fig. 2 Tapping mode scanning force microscopy images of OBs. **a** Amplitude image of OBs deposited onto hydrophilic substrate and (*inset*) typical section of a coalesced OBs. **b** Amplitude image of OBs deposited onto hydrophobic silicon substrate with (*inset*) typical height profile of OBs. **c** Amplitude image of a magnification (2×2 μm size) and **d** a further zoom of OBs patterned "monolayer" (1×1 μm size)

The thickness of single OBs is about 10 nm, also taking into account tip convolution in the calculation of round-shaped structures like our OBs (our SFM cantilever has a typical radius of curvature below 15 nm). OBs dimensions are variable between 50 and 200 nm. They are rather dense and uniform. This behavior is in agreement with reduction of Gibbs free energy: contact surface between solid support and OBs has to be minimized, leading to OBs spherical shape as observed in SFM images. By contrast, when the interaction is between two surfaces with similar features, the hydrophilic–hydrophilic interaction leads to OBs instability which results in the rapid coalescence of OBs (see Fig. 2a).

The differences found in OB morphology when patterned onto hydrophilic/hydrophobic substrates could be explained considering different interactions acting between the substrate and the surface of OBs. In particular, the silicon substrate interacts with the membrane of OBs, where the polar heads of phospholipids and the polar domains of some OB proteins are exposed [4, 5]. Oleosins, in particular, are the main proteins and play an important role

in the stability of OBs. They are amphiphatic proteins, even though they do not behave like membrane proteins, since they localize at a single lipid/water interface between the TAG core of OBs and the surrounding aqueous cytoplasm. Current models suggest that they are deeply inserted into the TAG core of OBs by the central hydrophobic domain, whereas the N- and C- hydrophilic termini of the protein protrude outside. The importance of the domains flanking the central hydrophobic domain in the OB stability was showed by Li and co-workers [18]. Indeed, OBs, reconstituted with the central hydrophobic domain of oleosin, showed a high tendency to coalesce, similar to that observed in OBs containing no oleosin, thus indicating that the central domain of this protein has a poor emulsifying and OB stabilizing features, whereas the surface-oriented N- and C-terminal domains could associate each other to form a tightly knitted amphipathic structure which stabilizes the entire OB.

OBs at the Air/Water Interface

Suspension of native and reconstituted OBs were injected underneath the water surface while monitoring surface pressure, the investigation of OBs behaviour of at the air/water interface has been performed following a two-step approach: monitoring of the variation of surface pressure vs. time, in other terms a kinetics experiment, and collection of images of the floating film originated on the sub-phase surface by Brewster angle microscopy (BAM) to gather information on the resulting film morphology.

The results of these experiments are described in Fig. 3 both for native (a) and reconstituted (b) OBs for sub-phases at neutral pH.

The first apparent and fundamental observation is the clear-cut change of surface pressure vs. time after OBs injection suggesting the formation of a surface-active layer at the air/water interface. Since the only perturbation to the system is the injection of OBs in the bulk of the sub-phase, it is natural to infer that OBs aggregates first diffuse in the bulk phase and then migrate at the interface. Hence, a remarkable and monitorable increase in surface pressure has been measured by the Wilhelmy balances just after injection with a typical pattern involving the immediate enhancement of pressure up to a plateau regime, generally around 15 mN/m. An evident example of such behaviour is illustrated in Fig. 3 ascribed to the injection of a suspension of OBs in the bulk of the water sub-phase at neutral pH.

It is noteworthy that the “response time” to the perturbation induced by the injection of OBs is remarkably fast. A possible mechanism could take into account a fast migration of the OB to the water surface followed by the formation of a surface film, this behaviour echoes the formation of lipid bilayers on solid surfaces upon vesicles disruption [19, 20]. Nevertheless, separate experiments (not shown here) demonstrated that the surface film can be compressed giving rise to a “pseudo” monolayer isotherm whose shape changes depending on the time allowed for equilibration after OB injection. Therefore, a simplistic view of OB disruption and formation of an adsorption layer of OB components has to be discarded although the increase in equilibrium surface pressure (see Fig. 3) is similar to the decrease in surface tension reported by other authors [9, 10] for adsorption monolayers of caleosin, i.e. 15–25 mN/m.

The morphology of the surface film formed at the air/water interface can be readily visualized by means BAM, a powerful technique usually utilised to monitor directly the morphology of floating layers at the air/water interface in the micron scale [21–23]. In the case of real interfaces, the intensity of the reflected radiation is mainly determined by the interfacial characteristics and evidences a minimum at the Brewster angle. Both the thickness of the floating layers and the roughness at the interface are critical parameters that determine the BAM images.

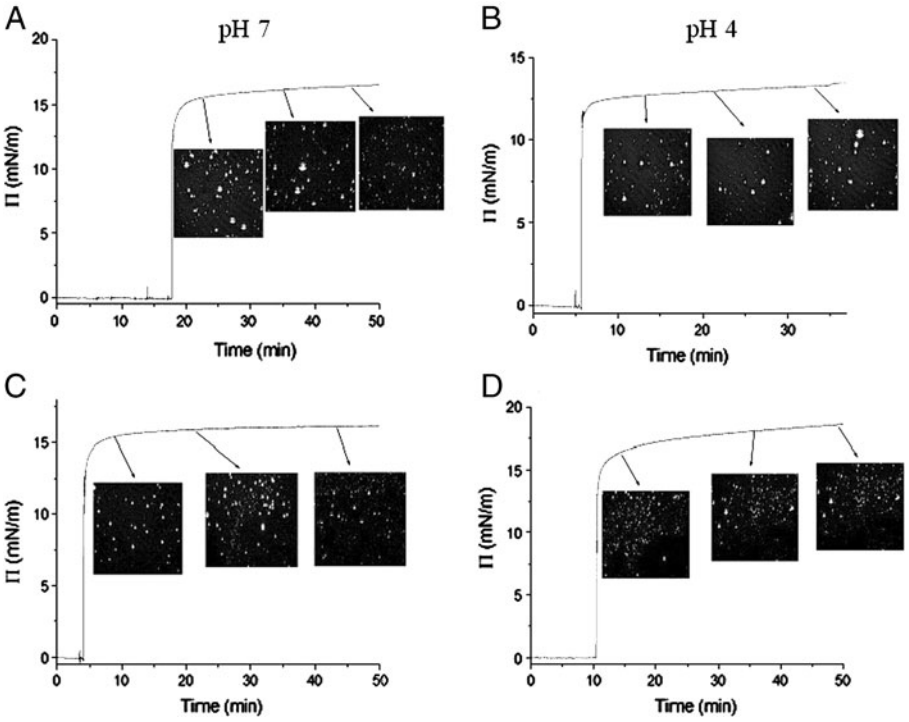

Fig. 3 BAM images of the floating film generated by native OBs (**a** and **b**) and reconstituted OBs (**c** and **d**). The images were taken at the following different surface pressure values in the plateau region: **a** 15.6, 16.1 and 16.4 mN/m; **b** 15.4, 15.8 and 16.1 mN/m. Sub-phase pH value of 7 in (a) and (c) and pH value of 4 in (b) and (d)

This method is expected to provide essential information about the presence of OBs and their aggregates in the surface film at the air/water interface.

BAM investigation was carried out along the plateau region of π-time isotherms and the corresponding snapshots are reported in Fig. 3, the images evidence a peculiar behaviour, more complex than first hypothesised in the light of the only kinetics curves and show the existence of a multiphasic film. All BAM images exhibit the simultaneous existence of both a three-dimensional (3D) domains of large and brilliant aggregates surrounded by a floating 2D film, probably monomolecular, which appears as a region only slightly more luminous than the black uncovered water surface. This finding suggests the formation of a fluid phospholipid monolayer where intact OBs or OBs aggregates can be dynamically embedded. This picture closely resembles what proposed for the arrangements of "water bodies" where the film at the water surface is visualized as organized into strata, with a very thin lipid layer overlaying a layer of proteins and polysaccharides [24, 25].

Moreover, BAM images show that 3D aggregates coalesce with time and become progressively larger and brighter; at the same time surface pressure remains practically constant in the plateau region, thus suggesting that the coalescence phenomenon is simultaneously accompanied by supplying of new OBs from the bulk of the aqueous sub-phase. Without such a dynamical process, the surface pressure at constant surface area should decrease. The same behaviour was observed for OBs reconstituted from the same seeds (Fig. 3b), thus indicating that reconstituted OBs have the same behaviour at the air/water interface than the native ones.

Previous studies on mixed monolayers of phosphatydilcholine and oleosin at the air/water interface report the presence of white diffuse stripes in BAM images due to protein segregation in the lipid layer [26]. Notably, such domains are not observed in the present work confirming that OB aggregates are mainly intact in the phospholipid film.

As shown in Fig. 3, no significant variations in this dynamic process were observed at different pH values (pH 4 and pH 7). This probably means that, in the experimental conditions here tested, the kinetics of coalescence of OBs at the air/water interface is not influenced by the pH value (similar images were obtained at pH 5 and pH 6; data not shown) and that the kinetics of bulk aggregation is much slower compared to migration and adsorption at the interface. Interestingly, the OBs surface charge density plays a minor role in governing the coalescence process in the fluid phospholipid matrix at the water/air interface.

OB ζ-potential

We investigated the surface charge properties of OBs reconstituted from almond and hazelnut seeds. At the tested conditions, the electrical charge of the two different preparations of OBs was similar. The recorded ζ-potential ranged from about −30 mV at pH 7 to +30 mV at pH 4 either in almond or hazelnut OBs (Fig. 4a and b). However, a slight change in the isoelectric point was observed, with the point of zero charge being around pH 5 in the case of hazelnut (Fig. 4a) and around pH 5–4 in the case of almond OBs

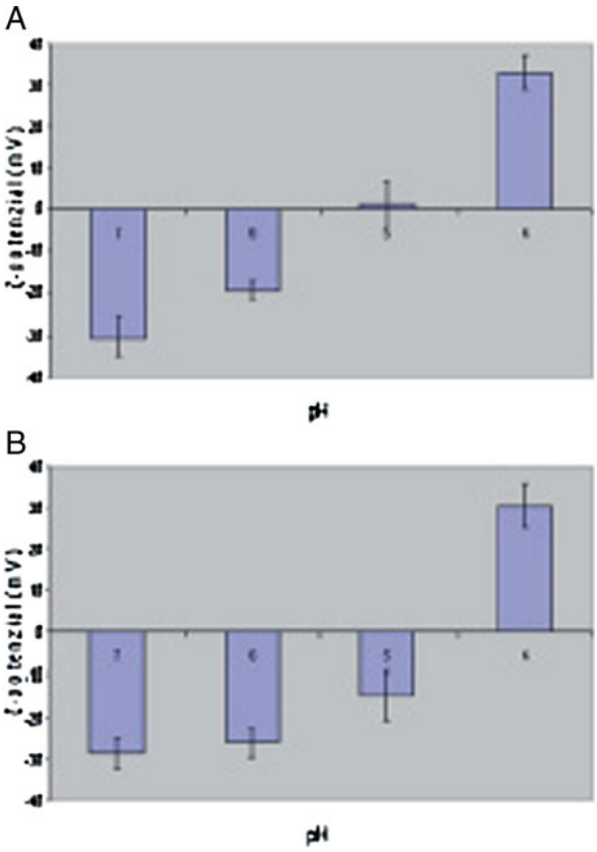

Fig. 4 ζ-potential values of OBs reconstituted from almond (C) and hazelnut (D) seeds

(Fig. 4b). A similar trend of ζ-potential at different pH values and similar isoelectric point was already reported for soybean OBs [27]. Therefore, at the neutral pH conditions used in the experiments shown in Fig. 4, OBs expose a negative charge on their surface and the interaction with an "unfavourable" substrate (hydrophilic as their outermost surface) most likely determines a shift in the OBs "equilibrium" shape.

OBs Uptake by Cancer Cells

FITC-loaded fluorescent OBs were used as markers to follow encapsulation and delivery into the MCF-7 breast cancer cell line. Cells were imaged after 4 h of treatment and stained by Phalloidin-TRITC (red fluorescence) to label the cytoskeleton (Fig. 5a). Figure 5b shows typical images of FITC loaded OBs uptaken by MCF-7 cancer cells. Overlapping these images allowed us to identify some different yellow spots derived from the merge of the fluorescence (Fig. 5c). Most of the internalized OBs showed a cytosolic localization with just few of them on the nuclear membrane. OBs internalization into cancer cells was also verified by confocal Z-scans images from different *x*–*y* plans. Similar uptake results were obtained with HeLa cells (data not shown).

Conclusions

In the present work, plant OBs were investigated by a combination of high-resolution techniques to elucidate their structure and their physicochemical properties. This approach

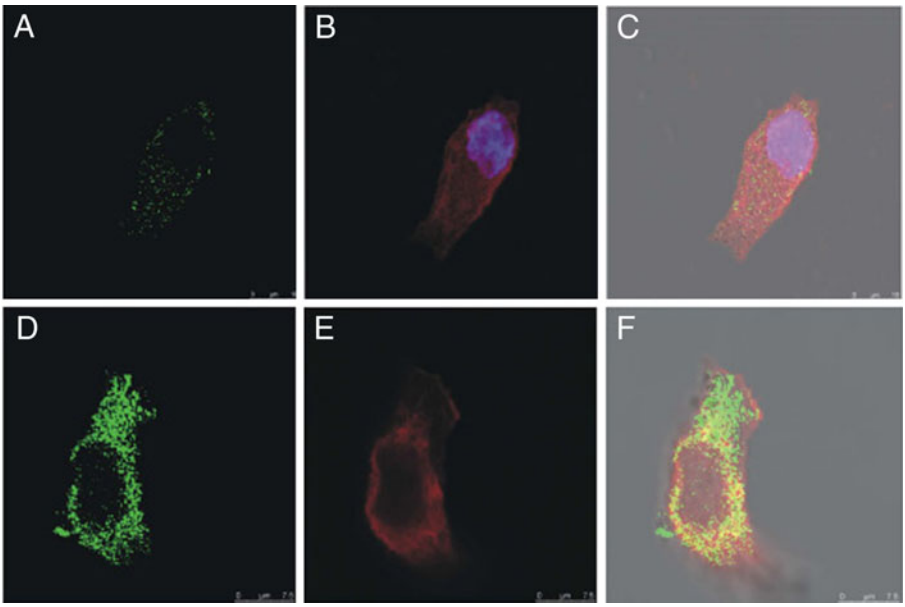

Fig. 5 CLSM micrographs showing the intracellular uptake of OBs into MCF-7. **a**–**d** FITC-loaded OBs internalised by MCF-7 cells; **b**–**e** MCF-7 cells cytoplasm stained with phalloidin-TRITC Fluorescence (*red*). In the case of image b, the nucleus was stained with Hoechst (*blue*); **c** FITC/Hoechst and phalloidin-TRITC fluorescences overlaid images

allowed us to demonstrate that OBs form stable ordered monolayers once transferred onto a hydrophobic substrates.

In order to use OBs as micro/nanocarriers to deliver lipophilic drugs, either FITC or CF was successfully loaded into OBs and used to follow their uptake by breast cancer cells. Taken together, our confocal results demonstrated that OBs are readily taken up by neoplastic cells and can be exploited as potential nanocarriers for loading and targeting natural bioactive compounds or anti-cancer drugs.

Acknowledgements We thank Mr. Luigi Dimo for assistance and performing all Langmuir experiments.

References

1. Bhatla, S. C., Kaushik, V., & Yadav, M. K. (2010). *Biotechnology Advances, 28*, 293–300.
2. Roberts, N. J., Scott, R. W., & Tzen, J. T. C. (2008). *Open Biotechnology Journal, 2*, 13–21.
3. Capuano, F., Beaudoin, F., Napier, J. A., & Shewry, P. R. (2007). *Biotechnology Advances, 25*, 203–206.
4. Fradsen, G. I., Mundy, J., & Tsen, J. T. C. (2001). *Physiologia Plantarum, 112*, 301–307.
5. Huang, A. H. C. (1996). *Plant Physiology, 110*, 1055–1061.
6. Huang, A. H. C. (1992). *Annual Review of Plant Physiology and Plant Molecular Biology, 43*, 177–200.
7. Chen, M. C. M., Chyan, C. L., Lee, T. T. T., Huang, S. H., & Tsen, J. T. C. (2004). *Journal of Agricultural and Food Chemistry, 52*, 3982–3987.
8. Peng, C. C., Lin, I. P., Lin, C. K., & Tsen, J. T. C. (2003). *Biotechnology Progress, 19*, 1623–1626.
9. Magrioti, V., Verger, R., & Constantinou-Kokotou, V. (2004). *Journal of Medicinal Chemistry, 47*, 288–291.
10. Purkrtova, Z., Le Bon, C., Karlova, B., Ropers, M. H., Anton, M., & Chardot, T. (2008). *Journal of Agricultural and Food Chemistry, 56*, 11217–11224.
11. Wang, L., Walsh, M. T., & Small, D. M. (2006). *PNAS, 103*, 6871–6876.
12. Santino, A., De Paolis, A., Gallo, A., Quarta, A., Casey, R., & Mita, G. (2003). *European Journal of Biochemistry, 270*, 4365–4375.
13. Hertz, H. (1981). *Journal fuer die Reine und Angewandte Mathematik, 92*, 156–171.
14. Johnson, K. L. (1985). *Contact mechanics*. Cambridge: Cambridge University Press.
15. Konig, D., & Mobius, D. (1991). *Journal of Physical Chemistry, 95*, 4590–4595.
16. He, Q., & Li, J. (2007). *Advances in Colloid Interface Science, 131*, 91–98.
17. Hunter, R. J. (1981). *Potential and colloid science*. New York: Academic.
18. Li, M., Murphy, D. J., Lee, K. K., Wilson, R., Smith, L. J., Clark, D. C., et al. (2002). *Journal of Biological Chemistry, 277*, 37888–37895.
19. Richter, R. P., Berat, R., & Brisson, A. R. (2006). *Langmuir, 22*, 3497–3505.
20. Castellana, T., & Cremer, P. S. (2006). *Surface Science Reports, 61*, 429–444.
21. Konig, D., & Mobius, D. (1991). *Journal of Physical Chemistry, 95*, 4590–4595.
22. He, Q., & Li, J. (2007). *Advances in Colloid Interface Sciences, 131*, 91–98.
23. Padamwar, M. N., & Pokharkar, V. B. (2006). *International Journal of Pharmaceutics, 320*, 37–44.
24. Wotton, R. S., & Preston, T. M. (2005). *Bioscience, 55*(2), 137–143.
25. Kozarac, Z., Mobiu, D., & Romero, M. T. M. (2000). *Water Research, 34*, 1463–1472.
26. Roux, E., Baumberger, S., Axelos, M. A. V., & Chardot, T. (2004). *Journal of Agricultural and Food Chemistry, 52*, 5245–5249.
27. Zhang, J., Chen, X. G., Peng, W. B., & Liu, C. S. (2008). Nanomedicine: nanotechnology. *Biology, and Medicine, 4*, 208–214.